



# Omens of coupled model biases in the CMIP5 AMIP simulations

Alina Găinușă-Bogdan<sup>1,2</sup> · Frédéric Hourdin<sup>1</sup> · Abdoul Khadre Traore<sup>1</sup> · Pascale Braconnot<sup>3</sup>

Received: 5 October 2016 / Accepted: 26 April 2017  
© Springer-Verlag GmbH Germany, part of Springer Nature 2017

## Abstract

Despite decades of efforts and improvements in the representation of processes as well as in model resolution, current global climate models still suffer from a set of important, systematic biases in sea surface temperature (SST), not much different from the previous generation of climate models. Many studies have looked at errors in the wind field, cloud representation or oceanic upwelling in coupled models to explain the SST errors. In this paper we highlight the relationship between latent heat flux (LH) biases in forced atmospheric simulations and the SST biases models develop in coupled mode, at the scale of the entire intertropical domain. By analyzing 22 pairs of forced atmospheric and coupled ocean-atmosphere simulations from the CMIP5 database, we show a systematic, negative correlation between the spatial patterns of these two biases. This link between forced and coupled bias patterns is also confirmed by two sets of dedicated sensitivity experiments with the IPSL-CM5A-LR model. The analysis of the sources of the atmospheric LH bias pattern reveals that the near-surface wind speed bias dominates the zonal structure of the LH bias and that the near-surface relative humidity dominates the east–west contrasts.

**Keywords** Climate model biases · AMIP simulations · Coupled simulations · Latent heat flux · Sea surface temperature · Sensitivity tests

## 1 Introduction

Most current coupled ocean-atmosphere global general circulation models suffer from important biases in the sea surface temperature (SST) fields over the tropical oceans, as shown in the coupled model inter-comparison project (CMIP) (Li and Xie 2012; Reichler and Kim 2008). These SST errors, affecting all tropical oceans, are mainly characterized by (1) an overly pronounced equatorial cold tongue that is too narrow, resulting in warm biases straddling the cold equatorial bias, and penetrates too far westward into the Pacific ocean (Mechoso et al. 1995; Szoeké and Xie 2008), (2) a warm bias located in the eastern part of the equatorial

Pacific and Atlantic oceans which, in the case of the Atlantic, leads to a weakening or reversal of the zonal SST gradient along the equator (Davey et al. 2002; Richter and Xie 2008) and (3) warm biases over the eastern tropical Pacific and Atlantic oceans (Richter 2015; Vanniere et al. 2014). A large number of coupled ocean-atmosphere models share these systematic SST errors and several studies have highlighted their persistence despite steady progress in climate modeling, physics and ocean-atmosphere coupling (Reichler and Kim 2008; Zheng et al. 2011; Xu et al. 2014a). The atmosphere models are very sensitive to the SST errors over the tropical oceans, thus limiting the reliability of coupled ocean-atmosphere model future projections for climate variability modes such as the Atlantic Niño or the West African monsoon (Batte and Deque 2011; Roehrig et al. 2013).

Some mechanisms were identified as potential sources of the SST errors in coupled models. Focusing on atmospheric causes, several studies have shown wind biases to be a driver of the erroneous ocean mean state (Chang et al. 2007; Szoeké and Xie 2008; Richter and Xie 2008; Wahl et al. 2011; Voldoire et al. 2014). Other studies have pointed out that atmospheric radiative biases, resulting from the difficulties of atmospheric models to adequately represent the low

✉ Frédéric Hourdin  
hourdin@lmd.jussieu.fr

<sup>1</sup> Laboratoire de Météorologie Dynamique/IPSL/UPMC Univ Paris 06/Sorbone Universités/CNRS, Paris, France  
<sup>2</sup> Environnements et Paléoenvironnements Océaniques et Continentaux/OASU/Université de Bordeaux/CNRS, Talence, France  
<sup>3</sup> Laboratoire des Sciences du Climat et de l'Environnement, IPSL, unité mixte CEA-CNRS-UVSQ, Gif sur Yvette, France

level atmospheric humidity and the strato-cumulus clouds, were the main source of the SST bias along the Atlantic African coast (Hu et al. 2011; Lin 2007). In an ocean-oriented view, other authors have emphasized the role of the ocean component that fails to correctly represent the coastal upwelling, as shown to be the case in the tropical Pacific by Zheng et al. (2011).

Recently, Hourdin et al. (2015) have identified the important role of the surface latent heat flux (LH) in forced atmospheric simulations, that shows an effect as strong as the cloud radiative effect in controlling the intensity of the eastern tropical warm bias in the CMIP5 simulations. They have found that, relative to the tropical mean, the models with the largest warm biases in the eastern tropical oceans in coupled mode are associated with the strongest regional surface incoming radiation and weakest regional evaporation in forced atmosphere mode. In particular, they highlighted a key role in the evaporation played by the near-surface relative humidity.

The aim of the present study is to go one step further in the analysis of the relationship between LH in the CMIP5 stand-alone atmospheric (AMIP) simulations and SST in the ocean-atmosphere coupled (CPL) simulations, this time, at the scale of the entire intertropical oceans domain. In Sect. 2, we analyze the CMIP5 simulations for the historical period and find a systematic correlation between the spatial patterns of the climatological LH biases in AMIP simulations and the climatological SST biases in CPL simulations. To highlight the link between these AMIP and CPL biases, we first decompose the LH bias in separate components due to biases in the associated state variables (Sect. 3.1) and then we complement the CMIP5 analysis with two sets of sensitivity experiments with the IPSL-CM5A-LR model, designed to focus on (1) how surface wind affects both AMIP LH and CPL SST (Sect. 3.2) and (2) how the local near-surface relative humidity affects the AMIP LH and in turn the CPL SST (Sect. 3.3). We summarize and discuss our findings in Sect. 4.

## 2 Parallel analysis of the CMIP5 AMIP and CPL historical simulations

### 2.1 Climatological surface fluxes and sea surface temperatures

This first section focuses on the joint analysis of pairs of CMIP5 (Taylor et al. 2012) historical coupled simulations (CPL) and atmospheric simulations forced with observational sea surface temperatures and sea ice cover (AMIP) (Taylor et al. 2000; Hurrell et al. 2008) performed with the same atmospheric general circulation model.

We consider climatologies of AMIP latent heat fluxes (LH—defined positive upwards) and CPL sea surface temperatures (SST) for the common period 1979–2005. The CMIP5 models for which both simulation outputs are available are listed in Table 1.

Our analysis focuses on the joint evaluation of the model climatological annual mean spatial patterns for these two variables over the intertropical oceans (30°S–30°N) against observational data. We use an ensemble of several in situ-based, satellite-based and blended flux products (Găinușă-Bogdan et al. 2015) and, after regridding both models and observational fields onto a common grid (that of the IPSL-CM5A-LR model), we calculate the climatological model biases with respect to each product for both AMIP LH and CPL SST. Since this results in similar large-scale bias features, here we show, for each model, the average of these different bias estimates.

Differences in model tuning can result in marked differences between the magnitudes of the variables considered here, as well as in differences in the relationship between the LH and SST bias magnitudes. As we do not focus on model tuning in this paper, we reduce its effect on our analyses by removing the mean bias over the study domain from the bias fields, thus obtaining what we will refer to as “bias pattern”:  $(M - O) - (\overline{M} - \overline{O})$ , where  $M$  stands for model field,  $O$  stands for observational field and the upper bar denotes a spatial average over our spatial domain. Removing the mean bias also avoids placing excessive confidence on the mean observational latent heat flux magnitudes, known to vary widely among observational products (WCRP 2000; Bourassa et al. 2008; Smith et al. 2011; Chaudhuri et al. 2013; Josey and Berry 2010; Gulev et al. 2010; Tomita et al. 2010; Kumar et al. 2012; Găinușă-Bogdan et al. 2015).

We find that, over wide regions, the SST bias patterns in many of the CMIP5 coupled simulations correspond to bias patterns of reversed sign in the LH fields of the forced atmospheric simulations. In other words, in regions where the atmospheric models develop relatively exaggerated surface latent heat fluxes under correct SST conditions, the coupled ocean-atmosphere models develop relatively cold sea surface biases and vice versa. This relationship is illustrated in Fig. 1, which shows the CMIP5 ensemble means for the AMIP LH and CPL SST bias patterns. This relationship, which suggests a direct and local influence of latent heat fluxes on SSTs is not surprising per se but the robustness of the relationship (further described in the following section) is indicative of a key process.

### 2.2 Characterization of the relationship between AMIP LH and CPL SST bias patterns

The relationship between the AMIP LH and CPL SST bias patterns differs in strength between models.

**Table 1** List of CMIP5 models included in this study

Model	Modeling center	References
ACCES1-0*	Commonwealth Scientific and Industrial Research Organization (CSIRO), Bureau of Meteorology (BOM)	Bi et al. (2013)
ACCES1-3*	CSIRO, BOM	Bi et al. (2013)
BCC-CSM1-1	Beijing Climate Center, China Meteorological Administration (BCC)	Xin et al. (2013)
BCC-CSM1-1-m	BCC	Xin et al. (2013)
BNU-ESM*	College of Global Change and Earth System Science (GCESS), Beijing Normal University	Ji et al. (2014)
CCSM4	National Center for Atmospheric Research (NCAR)	Gent et al. (2011)
CESM1-CAM5	National Science Foundation (NSF), Department of Energy (DOE), NCAR	Kay et al. (2015)
CMCC-CM	Centro Euro-Mediterraneo per I Cambiamenti Climatici (CMCC)	Scoccimarro et al. (2011)
CNRM-CM5*	Centre National de Recherches Météorologiques (CNRM), Centre Européen de Recherche et de Formation Avancée en Calcul Scientifique (CERFACS)	Voldoire et al. (2013)
CSIRO-Mk3-6-0*	Commonwealth Scientific and Industrial Research Organisation (CSIRO), Queensland Climate Change Centre of Excellence (QCCCE)	Jeffrey et al. (2013)
FGOALS-g2	State Key Laboratory of Numerical Modeling for Atmospheric Sciences and Geophysical Fluid Dynamics (LASG), Institute of Atmospheric Physics, Chinese Academy of Sciences (IAP), Center of Earth System Science, Tsinghua University (CESS)	Li et al. (2013)
FGOALS-s2*	LASG, IAP	Bao et al. (2013)
GFDL-CM3*	National Oceanic and Atmospheric Administration (NOAA), Geophysical Fluid Dynamics Laboratory (GFDL)	Griffies et al. (2011)
INMCM4	Institute for Numerical Mathematics	Volodin et al. (2010)
IPSL-CM5A-LR*	Institute Pierre-Simon Laplace (IPSL)	Dufresne et al. (2013)
IPSL-CM5A-MR	IPSL	Dufresne et al. (2013)
IPSL-CM5B-LR*	IPSL	Dufresne et al. (2013)
MIROC5*	Atmosphere and Ocean Research Institute (The University of Tokyo), National Institute for Environmental Studies, Japan Agency for Marine-Earth Science and Technology	Watanabe et al. (2010)
MPI-ESM-LR	Max Planck Institute for Meteorology (MPI-M)	Giorgetta et al. (2013)
MPI-ESM-MR	MPI-M	Giorgetta et al. (2013)
MRI-CGCM3*	Meteorological Research Institute (MRI)	Yukimoto et al. (2012)
NorESM1-M	Norwegian Climate Centre (NCC)	Bentsen et al. (2012)

Models marked with an asterisk are also included in the decomposition analysis in Sect. 3.1

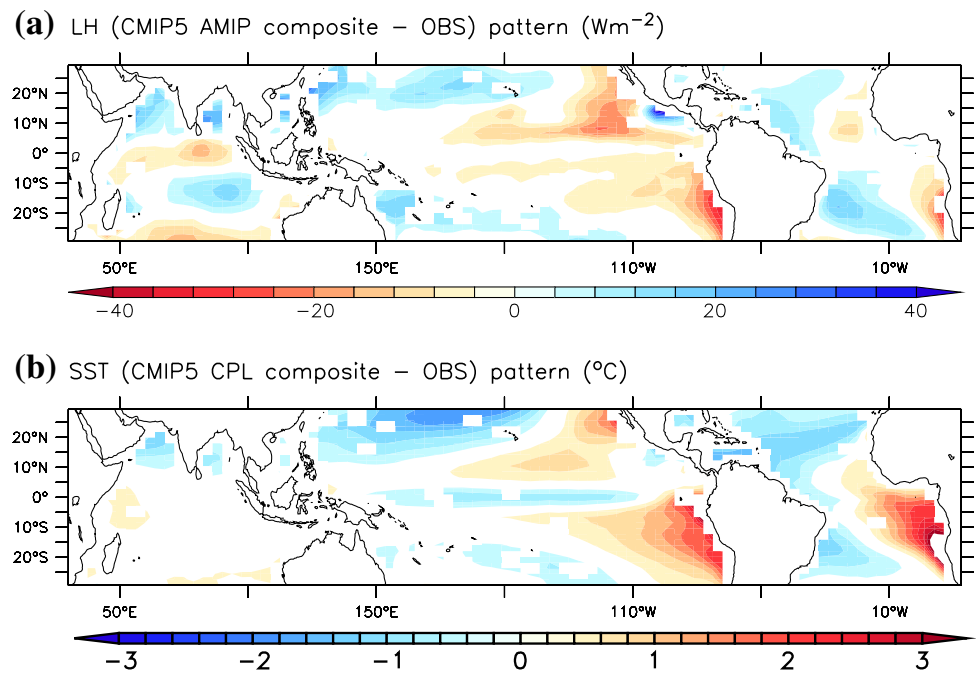
Figure 2a shows two measures of this relationship strength for each model. The top panel shows the interquartile ranges and medians for the ratios of the climatological AMIP LH to CPL SST bias patterns evaluated at each grid point (i.e., for the statistical distribution of  $[(LH_{AMIP} - LH_{OBS}) - \overline{(LH_{AMIP} - LH_{OBS})}] / [(SST_{CPL} - SST_{OBS}) - \overline{(SST_{CPL} - SST_{OBS})}]$  values over the intertropical oceans domain). The values of these ratios typically vary between  $-30$  and  $20 \text{ W/m}^2/\text{C}$ , but their medians are negative for all models, representative of the systematically inverse relationship between the large-scale AMIP LH and the CPL SST bias patterns. The medians of their ratios have an average of  $-7.2 \text{ W/m}^2/\text{C}$  and range from  $-2.5 \text{ W/m}^2/\text{C}$  for IPSL-CM5B-LR to  $-17.1 \text{ W/m}^2/\text{C}$  for CSIRO-Mk3-6-0.

The bottom panel in Fig. 2a shows the percent of the CPL SST bias pattern variance explained by the corresponding AMIP LH bias pattern for each model analyzed. This statistic is calculated as the squared norm of the projection of the CPL SST bias pattern field on the AMIP LH

bias pattern, divided by the squared norm of the CPL SST bias pattern (see “Appendix”), so that a perfect projection would correspond to 100% explained variance. This explained variance ranges from 3% for CESM1-CAM5 to 59% for FGOALS-s2. Note that: (1) there is no correlation between the bias pattern ratios (top panel of Fig. 2a—a measure of local magnitude of the relationship) and the explained variance (bottom panel of Fig. 2a—measure of pattern correspondence); (2) there is also no correlation between the median values of the bias pattern ratios (red lines on the top panel of Fig. 2a) and their spread (range of values spanned by the blue rectangles on the same figure) for each model. There is thus a great range of variability among the models in the relationship between the AMIP LH and the CPL SST bias patterns.

To illustrate the variability in spatial distributions among models, in Fig. 2b–d we show the pairs of AMIP LH and CPL SST bias patterns for three particular models:

**Fig. 1** Bias patterns for the CMIP5 composite: **a** forced atmospheric simulations latent heat flux; **b** coupled historical simulations sea surface temperature



- IPSL-CM5A-LR—found to have the sixth strongest AMIP LH - CPL SST bias relationship among the models considered (it is used for sensitivity experiments in Sects. 3.2 and 3.3);
- ACCESS1-3—found to have the sixth weakest relationship
- CSIRO-Mk3-6-0—the only one of the analyzed models to have a markedly different CPL SST bias pattern compared to the the CMIP5 composite shown in Fig. 1b; ranked 14 out of the 22 models in terms of their SST bias variance explained by the AMIP LH bias pattern.

Ignoring the mean biases and focusing solely on their patterns reveals very similar structures of opposite signs between the tropical AMIP LH and CPL SST biases in all three ocean basins in IPSL-CM5A-LR (Fig. 2b). For this model, the AMIP LH bias explains 33% of the spatial variance in the SST bias pattern (Fig. 2a).

Wide-spread correspondence of AMIP and CPL bias patterns is found for all models with higher or similar scores to IPSL-CM5A-LR in Fig. 2a. Even down to 23% explained variance, a pattern correspondence is apparent over most of the intertropical ocean basins, as seen for CSIRO-Mk3-6-0 in Fig. 2c. Even though the SST bias in this model bares some marked differences from most of the CMIP5 models (e.g., no warm bias in the south-east Pacific and Atlantic basins), the inverse AMIP LH - CPL SST bias pattern relationship still holds for wide areas over the Indian Ocean, the Pacific and the tropical South Atlantic. A notable exception, where relatively exaggerated atmospheric latent heat fluxes in the CSIRO-Mk-3-6-0 forced atmospheric model are not consistent with

the relatively overestimated coupled model SSTs in the present optic, is over the tropical North Atlantic (Fig. 2c).

Even for the models in the lower end of the AMIP LH - CPL SST bias relationship spectrum in Fig. 2a, the mark of this relationship is visible in certain regions. For example, for the sixth lowest ranked model, ACCESS1-3 (15% explained variance, Fig. 2a), the spatial signature of this relationship is virtually absent over most of the Pacific basin, but is visible in the tropical south-east Pacific coastal region and partly in the Indian and tropical Atlantic oceans (Fig. 2d).

A correspondence of sea surface temperature biases in coupled ocean-atmosphere simulations with the latent heat flux bias patterns in forced atmospheric simulations is thus found over a wide array of models.

### 3 Separating contributions to the latent heat flux biases

#### 3.1 Decomposition of the latent heat flux bias into its different atmospheric contributions

In order to identify the possible origins of the latent heat flux biases, we apply the decomposition of Hourdin et al. (2015). The latent heat flux reads:

$$LH = \rho L C_E |V_a| [\alpha q_{\text{sat}}(T_s) - q_a] \quad (1)$$

where  $\rho$  is the near-surface air density,  $L$  is the latent heat of vaporization,  $C_E$  is the bulk transfer coefficient for humidity,  $|V_a|$  is the near-surface wind velocity,  $q_{\text{sat}}(T_s)$  is the saturation humidity at the sea surface temperature,  $q_a$  is the

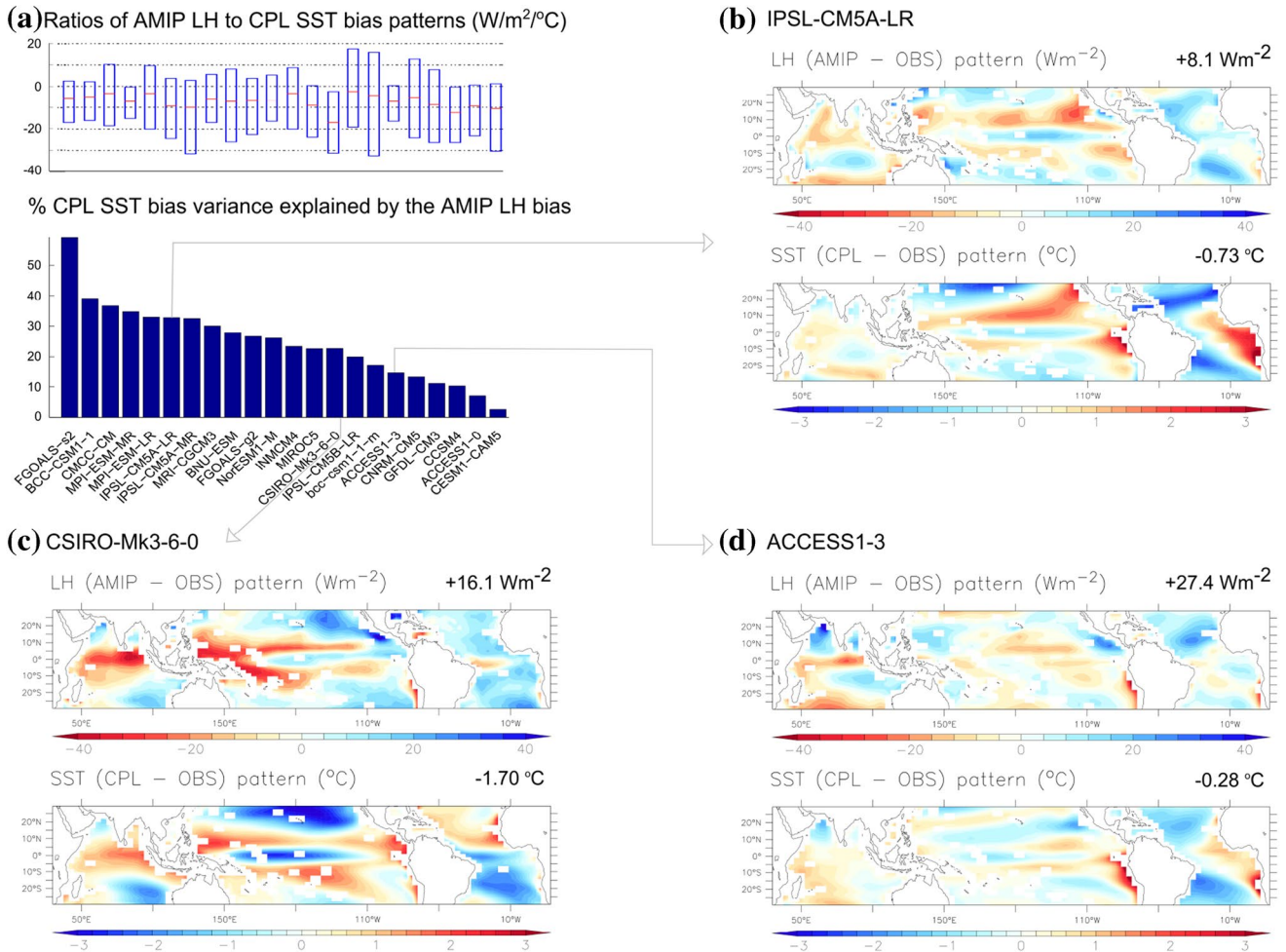


**Fig. 2** **a** Statistics describing the relationship between the AMIP LH and CPL SST bias patterns for 22 CMIP5 models—*top*: box plots representing the 25th and 75th percentiles (*box edges*) and medians (*red marks*) of the AMIP LH to CPL SST bias pattern ratios at every grid point over the intertropical oceans domain, *bottom*: percent of CPL SST bias pattern variance explained by the AMIP LH bias pat-

tern; examples of maps of AMIP LH and CPL SST bias patterns for: **b** IPSL-CM5A-LR; **c** CSIRO-Mk3-6-0; **d** ACCESS1-3. Values above *upper right corners* of maps represent the mean biases over the tropics that were subtracted from the full bias fields in order to obtain the patterns presented on the maps

near-surface specific air humidity and  $\alpha \approx 0.98$  is introduced in some models to take into account the smaller evaporative capacity of salty compared to fresh water.

By introducing the relative humidity  $RH = q_a/q_{sat}(T_a)$  and linearizing  $q_{sat}(T_s) - q_{sat}(T_a)$  as a function of  $\delta T = T_s - T_a$ , Eq. 1 for the latent heat flux reads:

$$LH = \gamma |V_a| \left[ \alpha \frac{\partial q_{sat}}{\partial T} (T=T_a) \delta T + (\alpha - RH) q_{sat}(T_a) \right] \quad (2)$$

with  $\gamma = \rho LC_E$ . When using the Clausius–Clapeyron equation:

$$\frac{\partial q_{sat}}{\partial T} (T=T_a) = \frac{Lq_{sat}(T_a)}{R_v T_a^2} \quad (3)$$

one obtains

$$LH = \gamma |V_a| q_{sat}(T_a) \left[ \alpha \frac{L\delta T}{R_v T_a^2} + \alpha - RH \right] \quad (4)$$

where  $R_v$  is the gas constant for water vapor. This formula is usually applied at each model time step, and  $T_a$  and  $RH_a$  correspond to the first model layer. Hourdin et al. (2015) show that the fluxes are well approximated by the above formula also when considering the climatological annual mean at standard observational levels, i.e., at 2 m for temperature and humidity  $T_a = T_{2m}$  and  $RH = RH_{2m}$ , and at 10 m for wind  $|V_a| = V_{10m}$ , if using an effective coefficient  $\gamma = 1.7 \times 10^{-3} \times 2.5 \times 10^6 \text{ J/m}^3$ .

The above formula can be differentiated with respect to variables  $|V_a|$ ,  $T_a$ ,  $\delta T$ , and  $RH$  to obtain the contribution of

the biases in these different variables to the latent heat flux bias:  $\Delta LH_{approx} = \Delta LH_{dyn} + \Delta LH_{Qsat} + \Delta LH_{RH} + \Delta LH_{\delta T}$ , with

$$\Delta LH_{dyn} = \gamma \Delta |V_a| q_{sat}(T_a) \left[ \alpha \frac{L\delta T}{R_v T_a^2} + \alpha - RH \right] \quad (5)$$

$$\Delta LH_{Qsat} = \gamma |V_a| \left\{ \frac{Lq_{sat}(T_a)}{R_v T_a^2} \left[ \alpha \frac{L\delta T}{R_v T_a^2} + \alpha - RH \right] - 2\alpha \frac{L\delta T}{R_v T_a^3} q_{sat}(T_a) \right\} \Delta T_a \quad (6)$$

$$\approx \gamma |V_a| q_{sat}(T_a) \frac{L}{R_v T_a^2} \left[ \alpha \delta T \left( \frac{L}{R_v T_a^2} - \frac{2}{T_a} \right) + \alpha - RH \right] \Delta T_a \quad (7)$$

$$\Delta LH_{RH} = -\gamma |V_a| q_{sat}(T_a) \Delta RH \quad (8)$$

$$\Delta LH_{\delta T} = \gamma |V_a| \times \alpha \frac{Lq_{sat}(T_a)}{R_v T_a^2} \Delta \delta T \quad (9)$$

For variables  $\Delta W_{10m}$ ,  $\Delta T_{2m}$  and  $\Delta \delta T_{2m} = \Delta(SST - T_{2m})$  we estimate the model bias as for LH, using the product ensemble compiled by Găinușă-Bogdan et al. (2015) (see Sect. 2.1). For  $RH_{2m}$  we use the da Silva et al. (1994) climatology.

Figure 3 presents the comparison between the actual AMIP LH bias pattern and the one approximated by the above decomposition, as well as the various terms of this decomposition for the ensemble mean of a subset of 11 models for which all necessary variables were available (models marked with an asterisk in Table 1). The figure shows both the ensemble mean of each term (left) and the ensemble standard deviation quantifying the inter-model dispersion around this mean (right). Note that the ensemble mean AMIP LH bias pattern in Fig. 3a is very similar to the full CMIP5 ensemble mean bias pattern in Fig. 1a, so that we may consider this sub-ensemble mean as representative of the CMIP5 ensemble.

Although not perfect, the decomposition allows to reproduce reasonably well the observed latent heat flux bias pattern. The LH bias pattern reconstructed from the decomposition terms,  $\Delta LH_{approx}$ , exaggerates the horizontal gradients of the observed multi-model mean bias pattern,  $\Delta LH$ , and the reconstructed inter-model spread of these patterns is larger than the one actually found in the subset of CMIP5 models. The reconstructed pattern also shows some differences in structure compared to the  $\Delta LH$  pattern in the central part of the tropical South Pacific. For all other regions, however, the spatial structures of the LH bias pattern are well captured in the reconstructed field. The agreement is in fact

surprising when considering that it is computed on an annual basis, with highly uncertain observations and ignoring the dependence of the drag coefficient to wind, temperature and humidity.

Out of the individual terms,  $\Delta LH_{dyn}$  and  $\Delta LH_{RH}$  clearly dominate the reconstructed LH bias. In contrast, the Clausius Clapeyron part is very weak because of the imposed sea surface temperature. The contribution of the surface— atmosphere temperature contrast is also small compared to the two dominant terms.

As was already discussed by Hourdin et al. (2015), the effect of relative humidity dominates the east–west contrasts, with a pattern which shares strong similarities with that of the mean CMIP5 SST biases. The effect of wind, which was not considered in the aforementioned paper, is more important on the center of oceanic basins and displays structures that are more elongated zonally. Interestingly, the inter-model dispersion for  $\Delta LH_{dyn}$  is very weak over the eastern side of the tropical oceans. Note that the effects of the wind and  $RH$  biases on  $\Delta LH$  can partially compensate each other in certain regions, most notably in the south-east tropical Pacific and Atlantic basins.

In Fig. 4 we show the same decomposition, this time applied on the AMIP LH bias of the IPSL-CM5A-LR model. The same comments can be made globally as for the ensemble discussed above. In the following, we use this model to demonstrate more directly, with sensitivity experiments, the impact of the wind and relative humidity biases on SSTs.

### 3.2 Wind-nudged simulations

In this section we explore the effect of the wind-induced latent heat flux biases by nudging the winds of the atmospheric model towards the ERA-Interim reanalysis (Dee et al. 2011) with a time constant of 3 h (see Coindreau et al. 2007 for more details). This essentially consists in adding a relaxation term towards the reanalysis fields in the model equations. Although not direct observations, the wind reanalyses contain observational information, especially reliable over the oceanic surface where wind is constrained by scatterometer observations. Note that, as shown in Găinușă-Bogdan et al. (2015), reanalyses tend to underestimate near-surface wind speed magnitudes compared to other observational products. However, the wind speed patterns, which are the focus of the present analysis, are consistent between reanalyses and other products, so reanalyses can successfully be used to correct model wind speed patterns.

The control (CTRL) and wind-nudged (WND) simulations are initialized from December 1979 conditions of a pre-existing historical IPSL-CM5A-LR simulation and are run for 20 years. They are performed in both coupled (CPL) and forced atmospheric (AMIP) model configurations and are compared to test to what extent wind nudging

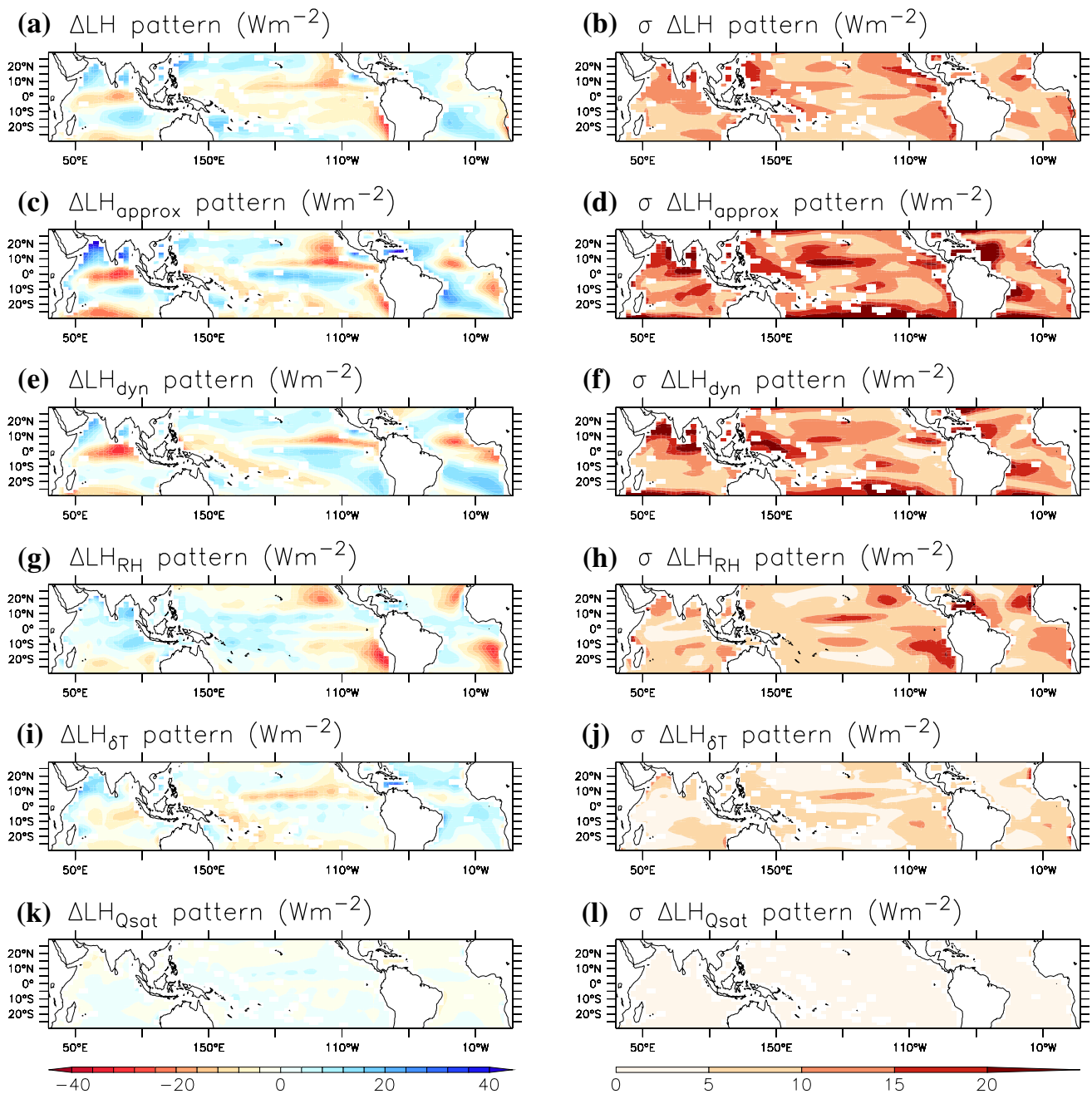


**Fig. 3** **a** Latent heat flux composite bias pattern for the 11-model CMIP5 sub-ensemble in AMIP configuration; **b** inter-model standard deviation of the AMIP LH bias patterns for the same sub-ensemble; **c–l** *left column*: sub-ensemble composites; *right column*: sub-ensemble standard deviations for the linear decomposition of the latent heat

flux bias patterns. **c, d** Total reconstructed bias pattern; **e, f** bias pattern associated to the wind speed bias; **g, h** bias pattern associated to the relative humidity bias; **i, j** bias pattern associated to the sea-air temperature contrast bias; **k, l** bias pattern associated to the saturation humidity bias

can correct the AMIP LH bias pattern and whether the same wind correction leads to an improvement in the CPL SST pattern.

Figure 5 shows the effects of the horizontal wind nudging on the AMIP near-surface wind speed and latent heat flux patterns (subfigures b and c), as well as on the CPL sea surface temperature pattern (subfigure d). The wind

nudging results in a partial correction of the AMIP LH bias pattern. The bias pattern amplitude, calculated as the standard deviation of the intertropical LH biases, decreases from 11 W/m<sup>2</sup> for the CTRL to 7 W/m<sup>2</sup> for the WND experiment. This difference is significant at the 99% confidence level if we consider the inter-observational spread. This AMIP LH pattern correction is consistent

**Fig. 4** Linear decomposition of the latent heat flux bias pattern in the IPSL-CM5A-LR AMIP simulation: **a** original bias pattern; **b** total reconstructed bias pattern; **c** bias pattern associated to the wind speed bias; **d** bias pattern associated to the relative humidity bias; **e** bias pattern associated to the sea-air temperature contrast bias; **f** bias pattern associated to the saturation humidity bias

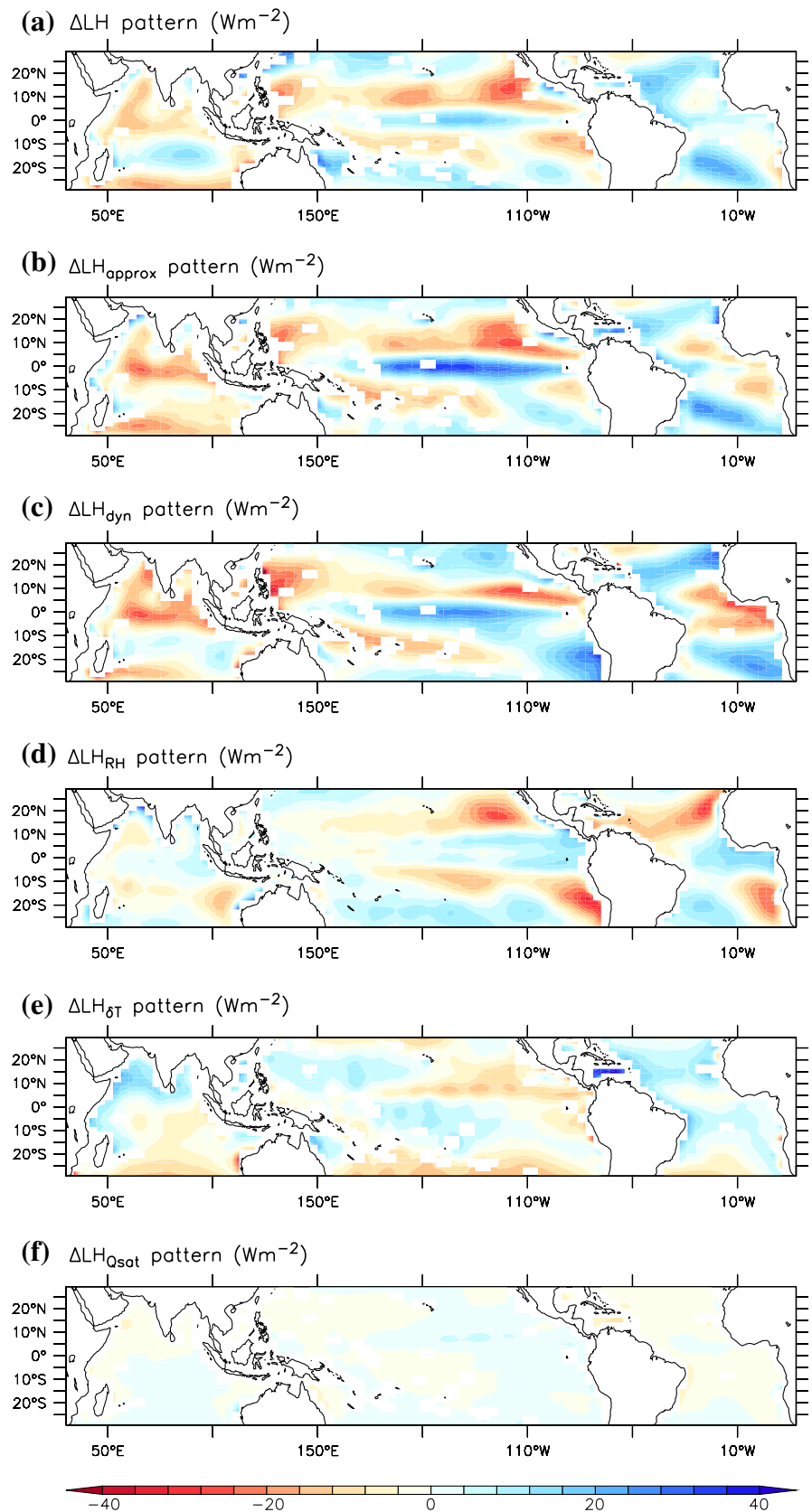
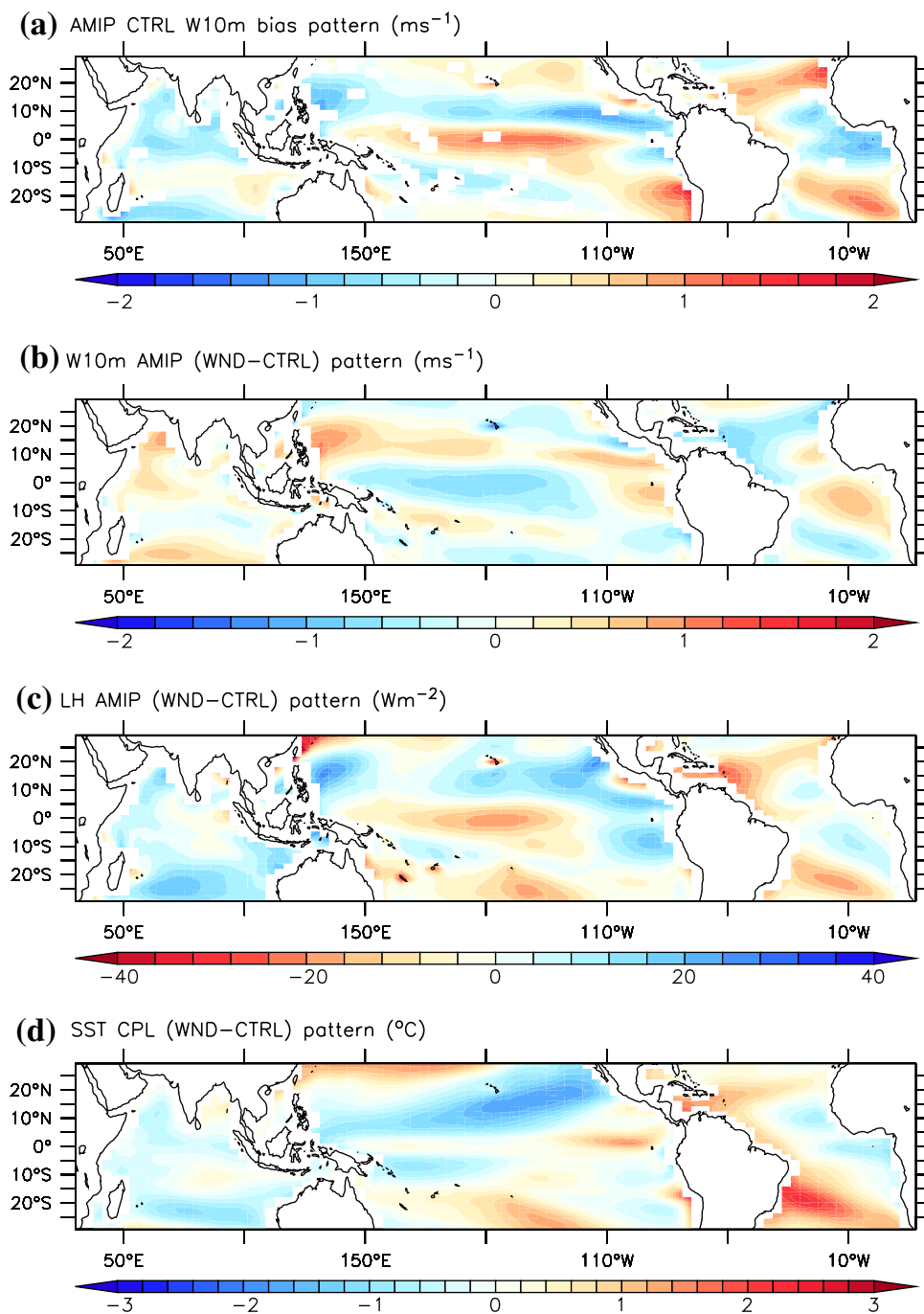


**Fig. 5** **a** 10 m-level wind speed bias pattern for the AMIP CTRL simulation; pattern differences between wind-nudged and control simulations for: **b** AMIP 10 m-level wind speed; **c** AMIP surface latent heat flux; **d** CPL sea surface temperature



with the W10m pattern difference between the WND and CTRL experiments: areas where the nudging results in relatively stronger wind typically show relatively stronger latent heat fluxes and vice-versa. The wind pattern change (Fig. 5b) explains 59% of the latent heat flux pattern change (Fig. 5c). Note that the spatial distribution of this AMIP LH pattern correction (Fig. 5c) matches to a great extent not just that of  $\Delta\text{LH}_{\text{dyn}}$  (Fig. 4c), but that of the full LH bias as well (Fig. 2b), once again highlighting the key

role of the wind speed representation on the latent heat flux in this model.

Applying the wind-nudging in the coupled IPSL-CM5A-LR model results in a modified sea surface temperature pattern compared to the CTRL simulation (Fig. 5d). A part of this response is certainly dynamically driven through the direct effect of the wind nudging on wind stress and, in turn, on the ocean dynamics. Nevertheless, the SST change (Fig. 5d) is to a large degree consistent with a response to the correction of the AMIP LH pattern (Fig. 5c), as

discussed above for the CMIP5 ensemble: regions where the latent heat fluxes are stronger in WND AMIP mode show relatively lower sea surface temperatures in WND CPL mode compared to the CTRL experiments (e.g., much of the Indian Ocean, subequatorial west Pacific, tropical north-east Pacific), and vice-versa (e.g., tropical-subtropical central and west Pacific, maximum trade wind regions in the Atlantic Ocean). Overall, the AMIP LH pattern correction explains 30% of the variance in the CPL SST pattern. The CPL SST bias is overall reduced in terms of pattern amplitude, from a standard deviation of the SST bias pattern of 1.1 °C in CTRL to 0.7 °C in the WND experiment (Fig. 6 vs. SST bias pattern in Fig. 2b).

### 3.3 Relative humidity-based correction of LH

The second major component of the LH bias is  $\Delta LH_{RH}$ , as shown in Fig. 4c.  $\Delta LH_{RH}$  explains a large part of the east–west  $\Delta LH$  contrasts. In this subsection, we attempt to synthetically correct the RH-related AMIP LH bias pattern and assess the impact that this has on the resulting CPL SST pattern.

In order to do so, we run a couple of AMIP (forced) and CPL (coupled), 20 year-long experiments with the IPSL-CM5A-LR model (initialized from an existing pre-industrial run) where, at each grid point over the tropics, we apply a time-independent  $\xi$  factor to the latent heat exchange coefficient used in the LH calculation (we will refer to these experiments as PERT). The specification of  $\xi$  is based on the following equation:

$$\xi LH_M = LH_M - \Delta LH_{RH} + \overline{\Delta LH_{RH}}, \quad (10)$$

where  $LH_M$  is the climatological average value of the simulated latent heat flux,  $\Delta LH_{RH}$  is the LH bias related to RH (Eq. 8; the RH bias is shown in Fig. 7a) and  $\overline{\Delta LH_{RH}}$  represents the  $\Delta LH$  averaged over the tropics (between 30°S and 30°N and 180°E and 180°W). The  $\xi$  factor can be seen as a correction factor (constant in time) applied on the exchange coefficient for latent heat flux, calibrated to correct LH from the effect of the annual mean bias pattern in relative humidity. For the sake of simplicity and in order to focus on this mean effect, we do not consider the seasonality of RH biases

in the definition of  $\xi$ , this sensitivity experiment aiming at demonstrating an effect, rather than at improving a model.

To highlight the effect of  $\xi$  on LH, Fig. 7b shows the normalized  $\xi$  field ( $\xi - 1$ ), in percent. Its pattern shows a significant east–west contrast, with maximum normalized  $\xi$  values over the eastern tropical oceans, consistent with the  $\Delta LH_{RH}$  pattern (Fig. 4d). A normalized local  $\xi$  factor of about 20% leads to a local change by more than 10 W/m<sup>2</sup> in the latent heat flux compared to the intertropical average in the forced atmospheric simulation, PERT AMIP (Fig. 7c). In this experiment, the AMIP LH pattern is strengthened both over the northern and southern east tropical oceans, but weakened along the equator. Applying this  $\xi$  factor results in a strong, systematic reduction of the AMIP RH-related LH bias pattern (Fig. 4d), correcting 7 out of its 9 W/m<sup>2</sup> of amplitude.

Once again, the change in the LH pattern between the AMIP simulation with the  $\xi$  parameter and the control is reflected in the resulting change of SST pattern between the corresponding coupled simulations, with 28% of the variance of the change in CPL SST pattern being explained by the change in the AMIP LH pattern. Over the eastern tropical oceans, this corresponds to a modification of the SST pattern on the order of 0.5–1 °C (Fig. 7d).

Note that the actual SST bias is not overall improved compared to the control experiment (Fig. 8 vs. Fig. 2b). The standard deviation of the PERT CPL SST bias pattern is, within the rounding error, the same as that of the control experiment (1.1 °C). This is partly because the change in SST is related to a partial, synthetic correction of not the full LH bias, but of a component of it (that associated to RH,  $\Delta LH_{RH}$ ), so that in the end its effect on the CPL SSTs is weak. Furthermore, because of the different (and sometimes opposed ways) in which the RH bias affects LH compared to the wind bias, in some regions a correction of the  $\Delta LH_{RH}$  pattern actually represents a worsening of the full LH bias pattern, since it adds to the wind-related bias. So while the associated SST pattern is improved in some regions, it is worsened in others by the perturbation in the LH calculation, so that at the scale of the tropics the PERT experiment does not result in a net improvement of the SST bias pattern.

**Fig. 6** Wind-nudged coupled IPSL-CM5A-LR sea surface temperature bias pattern

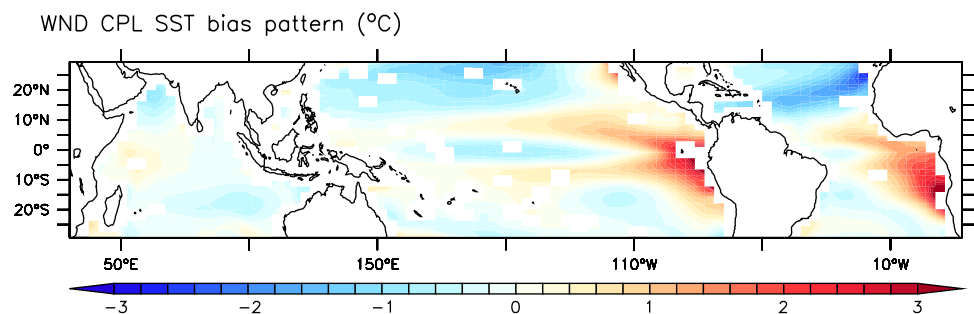
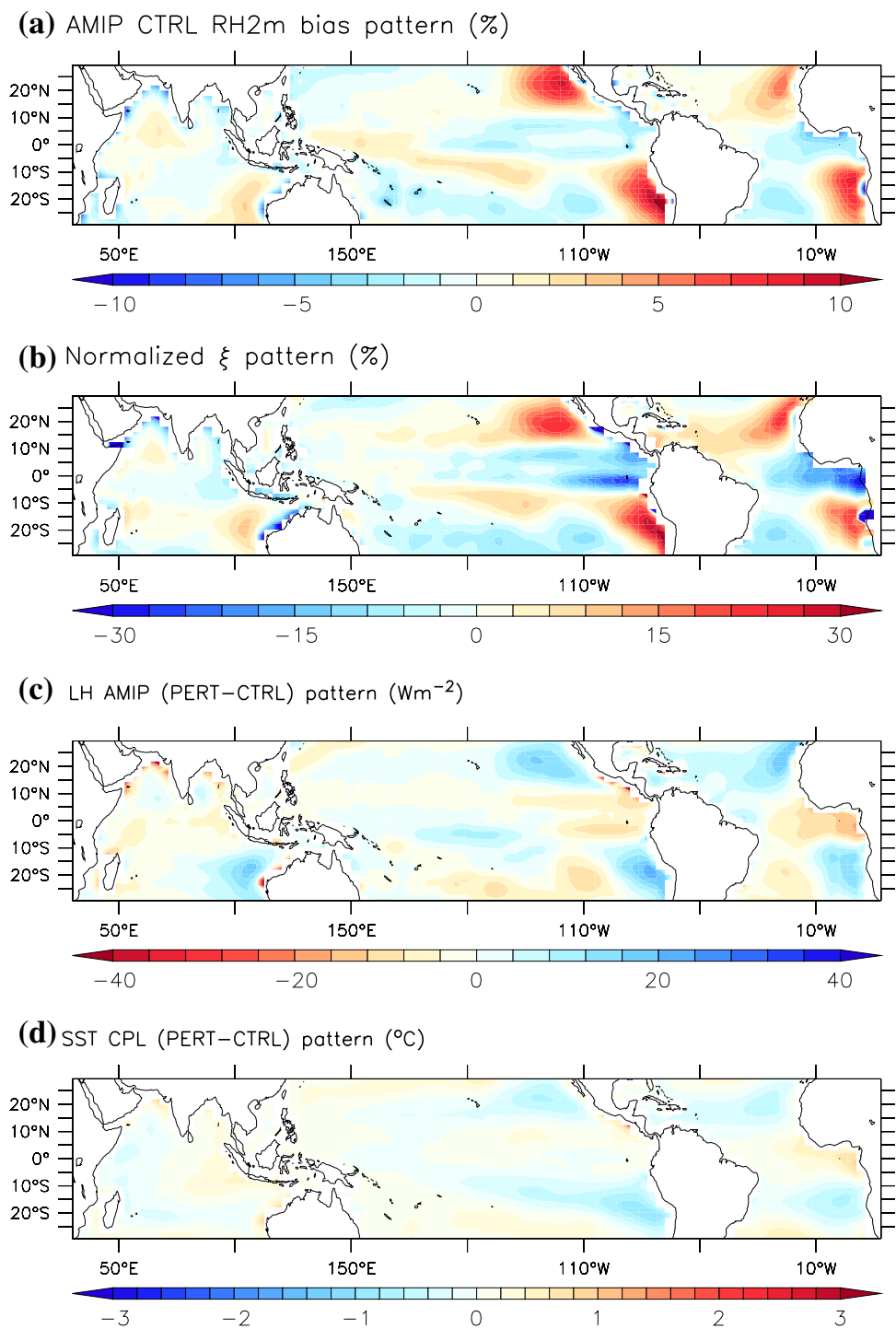


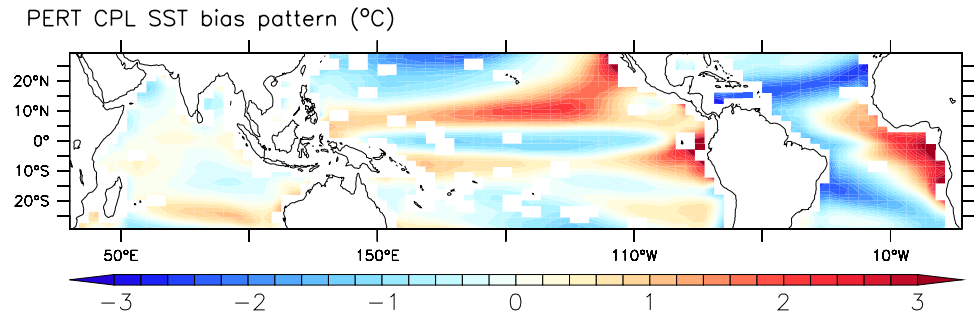
**Fig. 7** **a** AMIP CTRL near-surface relative humidity bias pattern; **b** normalized pattern of the  $\xi$  factor synthetically applied to the latent heat exchange coefficient in the PERT simulations; **c** pattern of the mean latent heat flux differences between the forced PERT and CTRL simulations; **d** pattern of the mean sea surface temperature differences between the coupled PERT and CTRL simulations



However, the purpose of these experiments is not to correct the SST bias pattern as such, but to test the coherence between the imposed LH pattern change in the AMIP experiment and the associated SST pattern response in CPL mode, and to highlight the potential specific role of the moist bias on the eastern warm biases. As in the previous analyses, the changes in CPL SST pattern are

indeed consistent with and of opposite sign compared to those in the AMIP LH pattern, indicating the same type of relationship between the latent heat flux in the forced atmospheric simulations and the sea surface temperature in coupled mode.

**Fig. 8** Sea surface temperature bias pattern of coupled simulation with  $\xi$  perturbation (PERT) performed with the IPSL-CM5A-LR model



## 4 Discussion

Robust results emerge from the above analyses.

First, the patterns of latent heat flux biases in stand-alone atmospheric simulations are systematically and negatively correlated with patterns of SST biases in the coupled simulations. This is true both at the individual scale for CMIP5 models and when considering sensitivity experiments with the IPSL-CM5A-LR model. The relationship between fluxes and SSTs is on average of the order of  $-7 \text{ W/m}^2/\text{°C}$ .

These results could have been expected. In the absence of other factors, a regionally-exaggerated/underestimated surface latent heat flux leads to excessive regional cooling/warming of the ocean surface and thus to an inverse pattern of SST bias. With an observationally-imposed SST field, errors in the atmospheric model reflect themselves on the distribution of other variables, such as the latent heat flux; when the SSTs are allowed to develop in the coupled model, the same atmospheric biases can express themselves in the SST field.

Because of the different energetic adjustment in the models, it is also not surprising that, even in the hypothetical scenario where atmospheric model LH biases were the main cause of the SST biases developed in the CPL models, there is not a 100% correspondence between the AMIP LH bias patterns and the CPL SST bias patterns. The correspondence of the large-scale AMIP and CPL bias structures over most of the domain distinguishable in Fig. 2b does not result in more than 33% explained variance partly because the localization of the structures is not exactly the same (shifts of spatial structures are expected when transitioning from forced to coupled systems) and partly because the magnitudes corresponding to these patterns are not linearly related, as other factors independent of the AMIP LH can influence the CPL SST. For individual models, this explained variance varies typically from 10 to 40%, and the mean regression from  $-5$  to  $-10 \text{ W/m}^2/\text{°C}$ .

It is worth reminding that comparing directly the LH biases in the coupled model with the SST biases would lead to a completely different and inextricable picture, the LH bias being generally dominated in coupled mode by the Clausius Clapeyron contribution  $\Delta LH_{Q_{\text{sat}}}$ , related to the SST bias, leading to overestimated evaporation over a too warm ocean surface and vice-versa.

Two major contributors are clearly identified to explain the latent heat biases.

Biases in relative humidity dominate the zonal gradients (east–west contrasts) over tropical oceans, and explain, probably in part, the classical and systematic warm bias over the region of stratocumulus, over the eastern tropical oceanic basins. An overestimated relative humidity at the surface in these regions reduces the surface evaporation, and thus the cooling of the oceanic surface. Based on a multi-model analysis, Hourdin et al. (2015) have already identified that the contribution to the warm bias of the reduced evaporation was as strong on average in the CMIP5 ensemble as the over-estimation of surface radiation due to a bad representation of stratocumulus clouds.

This direct impact of surface humidity biases on LH and SSTs which was deduced from an inter-model relationship in the CMIP5 ensemble is demonstrated here more directly with a sensitivity experiment with the IPSL-CM5A-LR model. When applying a correcting factor to the coupling coefficient that compensates for the error in the  $\alpha - RH$  factor in the LH decomposition, the expected effect is obtained both in AMIP LH and CPL SSTs, highlighting a local effect of relative humidity on LH and on SSTs, despite the interactions with the large-scale circulation (wind, water transport etc.). Note that there is an idea in the community that such an experience should not work because of compensating effects: an increased coupling coefficient would increase evaporation and then humidity, with a self limiting effect on evaporation. It is not the case when considering relative humidity, probably because relative humidity is to first order controlled by vertical mixing in the boundary layer.

Biases in surface wind also contribute strongly to the LH and SST biases. The effect is stronger than that of the RH biases on the west side of oceanic basins and is expressed in zonal structures rather than east–west contrasts. Here as well the multi-model results are confirmed by the sensitivity experiments with the IPSL-CM5A-LR model. Correcting the winds by nudging towards reanalysis fields directly impacts surface latent heat fluxes in forced atmospheric simulations and in turn (and in a correlated way) the SSTs in coupled mode. It results in our case in a reduction of the

SST biases in most of the tropical oceans, except for the eastern warm bias.

For the wind-nudging experiment, modifying the wind field acts on SSTs not only through latent heat but also through modification of the oceanic circulation. This effect could contribute to the correlation between latent heat modification in imposed-SST simulations and SST biases in coupled mode. However, such effect cannot be invoked for the RH experiments which clearly confirm the link between the modification of the LH field in forced atmospheric simulations and changes in the SST fields in coupled mode.

The goal of these sensitivity experiments was to demonstrate and quantify the effects of winds and relative humidity on SST biases through modifications of the latent heat flux, and show the potential for improvement that could occur from a better representation of atmospheric processes. Our results indicate that biases in atmospheric physics, and in particular in the boundary layer dynamics that strongly control the surface wind intensity and relative humidity, are of significant importance in the control of the air–sea coupling. This study suggests that new process studies and parameterization developments or improvements may help reduce the longstanding SST biases and that flux pattern evaluation in forced atmospheric simulations may be a powerful predictive tool for the SST bias development in fully coupled ocean–atmosphere models.

**Acknowledgements** We wish to thank Jean-Louis Dufresne for the fruitful discussions in the early stages of this work which have helped shape the CMIP5 analysis. We also wish to thank Lidia Mellul and Jérôme Servonnat for providing the wind-nudged simulations used in this study. We acknowledge the World Climate Research Programme's Working Group on Coupled Modelling, which is responsible for CMIP, and we thank the climate modeling groups (listed in Table 1 of this paper) for producing and making available their model output. For CMIP the U.S. Department of Energy's Program for Climate Model Diagnosis and Intercomparison provides coordinating support and led development of software infrastructure in partnership with the Global Organization for Earth System Science Portals. For the access and analysis of the CMIP5 data, we have benefited from the IPSL Prodiguier-Ciclad facility, supported by CNRS, UPMC, and Labex L-IPSL which is funded by the ANR (Grant ANR-10-LABX-0018) and by the European FP7 IS-ENES2 project (Grant 312979). The research leading to these results received funding from the EU FP7/2007-2013 under grant agreement no. 603521 and benefited as well from support of the ANR project "CONVERGENCE" (N8ANR-13-MONU-0008). Finally, we are extremely grateful to Olivier Boucher for providing financial support for this work through the MACC II project.

## Appendix: Computation of explained variance

In order to calculate the variance of pattern  $A$  (e.g., the CPL SST bias pattern) explained by pattern  $B$  (e.g., the AMIP LH bias pattern), we project pattern  $A$  on pattern  $B$ . We first normalise  $B$  so as to obtain a representative unit vector, perform

the vector projection and then compare the variance represented by this projection to the total variance of pattern  $A$ .

In practice, this consists of considering vectors  $\mathbf{a}$  and  $\mathbf{b}$  containing the ordered sequences of grid point values corresponding to  $A$  and  $B$ , respectively. We calculate the projection of  $\mathbf{a}$  on  $\mathbf{b}$ ,  $\mathbf{a}_b$ , as:

$$\mathbf{a}_b = (\mathbf{a} \cdot \hat{\mathbf{b}})\hat{\mathbf{b}}, \quad (11)$$

where

$$\hat{\mathbf{b}} = \frac{\mathbf{b}}{\|\mathbf{b}\|}. \quad (12)$$

We then calculate the associated proportion of explained variance as the squared norm of the projection divided by the squared norm of  $\mathbf{a}$ , i.e.,  $\frac{\|\mathbf{a}_b\|^2}{\|\mathbf{a}\|^2}$ .

This process is mathematically equivalent to calculating  $\frac{(\mathbf{a} \cdot \mathbf{b})^2}{(\mathbf{a} \cdot \mathbf{a})(\mathbf{b} \cdot \mathbf{b})}$ .

## References

- Bao S, Lin P, Zhou T, Liu Y, Yu Y, Wu G, He B, He J, Li L, Li J, Li Y, Liu H, Qiao F, Song Z, Wang B, Wang J, Wang P, Wang X, Wang Z, Wu B, Wu T, Xu Y, Yu H, Zhao W, Zheng W, Zhou L (2013) The flexible global ocean–atmosphere–land system model, Spectral Version 2: FGOALS-s2. *Adv Atmos Sci* 30(3):561–576
- Batte L, Deque M (2011) Seasonal predictions of precipitation over Africa using coupled ocean–atmosphere general circulation models: skill of the ENSEMBLES project multimodel ensemble forecasts. *Tellus-A* 63:283–299. doi:10.1111/j.1600-0870.2010.00493.x
- Bentsen M, Bethke I, Debernard JB, Iversen T, Kirkevåg A, Seland Ø, Drange H, Roelandt C, Seierstad IA, Hoose C, Kristjánsson JE (2012) The Norwegian earth system model, NorESM1-M. Part 1: Description and basic evaluation. *Geosci Model Dev Discuss* 5:28432931
- Bi D, Dix M, Marsland S, O'Farrell S, Rashid H, Uotila P, Hirst T, Kowalczyk E, Golebiewski M, Sullivan A, Yan H, Hannah N, Sun CFZ, Vohralik P, Watterson I, Zhou X, Fiedler R, Collier M, Ma Y, Noonan J, Stevens L, Uhe P, Zhu H, Griffies S, Hill R, Harris C, Puri K (2013) The ACCESS coupled model: description, control climate and evaluation. *Aust Meteorol Oceanogr J* 63:41–64
- Bourassa MA, Hughes PJ, Smith SR (2008) Surface turbulent flux product comparison. *Flux Netw* 5:22–24
- Chang C, Carton J, Grodsky S, Nigam S (2007) Seasonal climate of the tropical Atlantic sector in the NCAR community climate system model 3: error structure and probable causes of errors. *J Clim* 20:1053–1070
- Chaudhuri AH, Ponte RM, Forget G, Heimbach P (2013) A comparison of atmospheric reanalysis surface products over the ocean and implications for uncertainties in air–sea boundary forcing. *J Clim* 26(1):153–170
- Coindreau O, Hourdin F, Haefelin M, Mathieu A, Rio C (2007) A global climate model with stretchable grid and nudging: a tool for assesment of physical parametrizations 135:1474–1489
- da Silva A, Young AC, Levitus S (1994) Atlas of surface marine data 1994, volume 1.: Algorithms and procedures. Tech. Rep. 6, U.S. Department of Commerce, NOAA, NESDIS

- Davey M, Huddlestone M, Sperber K, Braconnot P, Bryan F, Chen D, Colman R, Cooper C, Cubasch U, Delecluse P, DeWitt D, Fairhead L, Flato G, Gordon C, Hogan T, Ji M, Kimoto M, Kitoh A, Knutson T, Latif M, Treut HL, Li T, Manabe S, Mechoso C, Meehl G, Power S, Roeckner E, Terray L, Vintzileos A, Washington RVBWW, Yoshikawa I, Yu JY, Yukimoto S, Zebiak S (2002) STOIC: a study of coupled model climatology and variability in tropical ocean regions. *Clim Dyn* 18:403–420. doi:[10.1007/s00382-001-0188-6](https://doi.org/10.1007/s00382-001-0188-6)
- Dee DP, Uppala SM, Simmons AJ, Berrisford P, Poli P, Kobayashi S, Andrae U, Balmaseda MA, Balsamo G, Bauer P, Bechtold P, Beljaars ACM, van de Berg L, Bidlot J, Bormann N, Delsol C, Dragani R, Fuentes M, Geer AJ, Healy LHSB, Hersbach H, Holm EVH, Isaksen I, Källberg PK, Köhler M, Matricardi M, McNally AP, Monge-Sanz BM, Morcrette JJ, Park BK, Peubey C, de Rosnay P, Tavolato C, Thépaut JN, Vitart F (2011) The ERA-Interim reanalysis: configuration and performance of the data assimilation system. *Q J R Meteorol Soc* 137:553–597
- Dufresne JL, Foujols MA, Denvil S, Caubel A, Marti O, Aumont O, Balkanski Y, Bekki S, Bellenger H, Benshila R, Bony S, Bopp L, Braconnot P, Brockmann P, Cadule P, Cheruy F, Codron F, Cozic A, Cugnet D, de Noblet N, Duvel JP, Ethé C, Fairhead L, Fichefet T, Flavoni S, Friedlingstein P, Grandpeix JY, Guez L, Guilyardi E, Hauglustaine D, Hourdin F, Idelkadi A, Ghattas J, Joussaume S, Kageyama M, Krinner G, Labetoulle S, Lahellec A, Lefebvre MP, Lefevre F, Levy C, Li ZX, Lloyd J, Lott F, Madec G, Mancip M, Marchand M, Masson S, Meurdesoif Y, Mignot J, Musat I, Parouty S, Polcher J, Rio C, Schulz M, Swingedouw D, Szopa S, Talandier C, Terray P, Viovy N, Vuichard N (2013) Climate change projections using the IPSL-CM5 earth system model: from CMIP3 to CMIP5. *Clim Dyn* 40(9–10):2123–2165
- Gent PR, Danabasoglu G, Donner LJ, Holland MM, Hunke EC, Jayne SR, Lawrence DM, Neale RB, Rasch PJ, Vertenstein M, Worley PH, Yang ZL, Zhang M (2011) The community climate system model version 4. *J Clim* 24(19):4973–4991. doi:[10.1175/2011JCLI4083.1](https://doi.org/10.1175/2011JCLI4083.1)
- Giorgetta M, Jungclaus J, Reick C, Legutke S, Bader J, Böttinger M, Brovkin V, Cruieger T, Esch M, Fieg K, Glushak K, Gayler V, Haak H, Hollweg HD, Ilyina T, Kinne S, Kornbluh L, Matei D, Mauritsen T, Mikolajewicz U, Mueller W, Notz D, Pithan F, Raddatz T, Rast S, Redler R, Roeckner E, Schmidt H, Schnur R, Segschneider J, Six K, Stockhause M, Timmreck C, Wegner J, Widmann H, Wieners KH, Claussen M, Marotzke J, Stevens B (2013) Climate and carbon cycle changes from 1850 to 2100 in MPI-ESM simulations for the coupled model intercomparison project phase 5. *J Adv Model Earth Syst* 5:572–597
- Griffies SM, Winton M, Donner LJ, Horowitz LW, Downes SM, Farneti R, Gnanadesikan A, Hurlin WJ, Lee HC, Liang Z, Palter JB, Samuels BL, Wittenberg AT, Wyman BL, Yin J, Zadeh N (2011) The GFDL CM3 coupled climate model: characteristics of the ocean and sea ice simulations. *J Clim* 24(13):3520–3544. doi:[10.1175/2011JCLI3964.1](https://doi.org/10.1175/2011JCLI3964.1)
- Găinușă-Bogdan A, Braconnot P, Servonnat J (2015) Using an ensemble data set of turbulent air-sea fluxes to evaluate the ipsl climate model in tropical regions. *J Geophys Res Atmos* 120(10):4483–4505. doi:[10.1002/2014JD022985](https://doi.org/10.1002/2014JD022985)
- Gulev SK, Josey SA, Bourassa M, Breivik LA, Cronin MF, Fairall C, Gille S, Kent EC, Lee CM, McPhaden MJ, Monteiro PMS, Schuster U, Smith SR, Trenberth KE, Wallace D, Woodruff SD (2010) Surface energy, CO<sub>2</sub> fluxes and sea ice. In: Hall J, Harrison DE, Stammer D (eds) *Proceedings of OceanObs'09: sustained ocean observations and information for society*. ESA Publication WPP-306, Venice
- Hourdin F, Frdric, Găinușă-Bogdan A, Braconnot P, Dufresne JL, Traore A, Rio C (2015) Air moisture control on ocean surface temperature, hidden key to the warm bias enigma. *Geophys Res Lett* 42(24):10,885–10,893. doi:[10.1002/2015GL066764](https://doi.org/10.1002/2015GL066764)
- Hu Z, Huang B, Hou Y, Wang W, Yang F, Stan C, Schneider E (2011) Sensitivity of tropical climate low-level clouds in the NCEP climate forecast system. *J Clim* 36:1795–1811. doi:[10.1007/s00382-010-0797-z](https://doi.org/10.1007/s00382-010-0797-z)
- Hurrell JW, Hack JJ, Shea D, Caron JM, Rosinski J (2008) A new sea surface temperature and sea ice boundary dataset for the communityatmosphere model. *J Clim* 21:5145–5153
- Jeffrey SJ, Rotstain LD, Collier MA, Dravitzki SM, Hamalainen C, Moeseneder C, Wong KK, Syktus JI (2013) Australia's CMIP5 submission using the CSIRO Mk3.6 model. *Aust Meteorol Oceanogr* 63:1–13
- Ji D, Wang L, Feng J, Wu Q, Cheng H, Zhang Q, Yang J, Dong W, Dai Y, Gong D, Zhang RH, Wang X, Liu J, Moore JC, Chen D, Zhou M (2014) Description and basic evaluation of Beijing Normal University Earth System Model (BNU-ESM) version 1. *Geosci Model Dev* 7(5):2039–2064. doi:[10.5194/gmd-7-2039-2014](https://doi.org/10.5194/gmd-7-2039-2014)
- Josey SA, Berry DI (2010) Air-sea fluxes of heat and freshwater. In: *MCCIP Annual Report Card 2010-11*, MCCIP Science Review
- Kay JE, Deser C, Phillips A, Mai A, Hannay C, Strand G, Arblaster JM, Bates SC, Danabasoglu G, Edwards J, Holland M, Kushner P, Lamarque JF, Lawrence D, Lindsay K, Middleton A, Munoz E, Neale R, Oleson K, Polvani L, Vertenstein M (2015) The community earth system model (CESM) large ensemble project: a community resource for studying climate change in the presence of internal climate variability. *Bull Am Meteorol Soc* 96(8):1333–1349. doi:[10.1175/BAMS-D-13-00255.1](https://doi.org/10.1175/BAMS-D-13-00255.1)
- Kumar BP, Vialard J, Lengaigne M, Murty VSN, McPhaden MJ (2012) TropFlux: air-sea fluxes for the global tropical oceans-description and evaluation. *Clim Dyn* 38(7–8):1521–1543
- Li G, Xie SP (2012) Origins of tropical-wide sst biases in cmip multi-model ensembles. *Geophys Res Lett* 39(22). doi:[10.1029/2012GL053777](https://doi.org/10.1029/2012GL053777)
- Li L, Lin P, Yu Y, Wang B, Zhou T, Liu L, Liu J, Bao Q, Xu S, Huang W, Xia K, Pu Y, Dong L, Shen S, Liu Y, Hu N, Liu M, Sun W, Shi X, Zheng W, Wu B, Song M, Liu H, Zhang X, Wu G, Xue W, Huang X, Yang G, Song Z, Qiao F (2013) The flexible global ocean-atmosphere-land system model. Grid-point Version 2: FGOALS-g2. *Adv Atmos Sci* 30(3):543–560. doi:[10.1007/s00376-012-2140-6](https://doi.org/10.1007/s00376-012-2140-6)
- Lin JL (2007) The double-ITCZ problem in IPCC AR4 coupled GCMs: ocean-atmosphere feedback analysis. *J Clim* 20:4497–4525. doi:[10.1175/JCLI4272.1](https://doi.org/10.1175/JCLI4272.1)
- Mechoso CR, Robertson A, Barth N, Davey M, Delecluse P, Gent P, Ineson S, Kirtman B, Latif M, Treut HL (1995) The seasonal cycle over the tropical Pacific in coupled ocean-atmosphere general circulation models. *Mon Weather* 9(123):2825–2838. doi:[10.1175/1520-0493\(1995\)9<2825>2.0.CO;2](https://doi.org/10.1175/1520-0493(1995)9<2825>2.0.CO;2)
- Reichler T, Kim J (2008) How well do coupled models simulate today's climate? *Bull Am Meteorol Soc* 89(303). doi:[10.1175/BAMS-89-3-303](https://doi.org/10.1175/BAMS-89-3-303)
- Richter I (2015) Climate model biases in the eastern tropical oceans: causes, impacts and ways forward. *Clim Change* 6:345–358. doi:[10.1002/wcc.338](https://doi.org/10.1002/wcc.338)
- Richter I, Xie SP (2008) On the origin of equatorial Atlantic biases in coupled general circulation models. *Clim Dyn* 31:587–598. doi:[10.1007/s00382-008-0364-z](https://doi.org/10.1007/s00382-008-0364-z)
- Roehrig R, Bouniol D, Guichard F, Hourdin F, Redelsperger JL (2013) The present and future of the west african monsoon: a process-oriented assessment of cmip5 simulations along the amma transect. *Clim Dyn* 26:6471–6505. doi:[10.1175/JCLI-D-12-00505.1](https://doi.org/10.1175/JCLI-D-12-00505.1)
- Scoccimarro E, Gualdi S, Bellucci A, Sanna A, Fogli PG, Manzini E, Vichi M, Oddo P, Navarra A (2011) Effects of tropical cyclones on ocean heat transport in a high resolution coupled general circulation model. *J Clim* 24:4368–4384

- Smith SR, Hughes PJ, Bourassa MA (2011) A comparison of nine monthly air–sea flux products. *Int J Climatol* 31(7):1002–1027
- Szoeke SD, Xie SP (2008) The tropical eastern Pacific seasonal cycle: assessment of errors and mechanisms in IPCC AR4 coupled ocean-atmosphere general circulation models. *J Clim* 21:2573–2590. doi:[10.1175/2007JCLI1975.1](https://doi.org/10.1175/2007JCLI1975.1)
- Taylor KE, Williamson D, Zwiers F (2000) The sea surface temperature and sea-ice concentration boundary conditions for AMIP II simulations. PCMDI report 60, Program for Climate Model Diagnosis and Intercomparison, Lawrence Livermore National Laboratory, Livermore, California
- Taylor KE, Stouffer RJ, Meehl GA (2012) An overview of CMIP5 and the experiment design. *Bull Am Meteorol Soc* 93(4):485–498
- Tomita H, Kubota M, Cronin MF, Iwasaki S, Konda M, Ichikawa H (2010) An assessment of surface heat fluxes from J-OFURO2 at the KEO and JKEO sites. *J Geophys Res* 115(C03):018
- Vanniere BE, Guilyardi E, Toniazzo T, Madec G, Woolhough S (2014) A systematic approach to identify the sources of tropical SST errors in coupled models using the adjustment of initialised experiments. *Clim Dyn* 43:2261–2282. doi:[10.1007/s00382-014-2051-6](https://doi.org/10.1007/s00382-014-2051-6)
- Voltaire A, Sanchez-Gomez E, Méliá DS, Decharme B, Cassou C, Sénési S, Valcke S, Beau I, Alias A, Chevallier M, Déqué M, Deshayes J, Douville H, Fernandez E, Madec G, Maisonnave E, Moine MP, Planton S, Saint-Martin D, Szopa S, Tyteca S, Alkama R, Belamari S, Braun A, Coquart L, Chauvin F (2013) The CNRM-CM5.1 global climate model: description and basic evaluation. *Clim Dyn* 40(9):2091–2121
- Voltaire A, Claudon M, Caniaux G, Giordani H, Roebrig R (2014) Are atmospheric biases responsible for the tropical Atlantic SST biases in the CNRM-CM5 coupled model? *Clim Dyn* 43(11):2963–2984
- Volodin EM, Dianskii NA, Gusev AV (2010) Simulating present-day climate with the INMCM4.0 coupled model of the atmospheric and oceanic general circulations. *Izvestiya, Atmospheric and Oceanic Physics* 46(4):414–431. doi:[10.1134/S000143381004002X](https://doi.org/10.1134/S000143381004002X)
- Wahl S, Latif M, Park W, Keenlyside N (2011) On the tropical Atlantic SST warm bias in the Kiel climate model. *Clim Dyn* 36:891–906
- Watanabe M, Suzuki T, Oishi R, Komuro Y, Watanabe S, Emori S, Takemura T, Chikira M, Ogura T, Sekiguchi M, Takata K, Yamazaki D, Yokohata T, Nozawa T, Hasumi H, Tatebe H, Kimoto M (2010) Improved Climate Simulation by MIROC5: Mean States, Variability, and Climate Sensitivity. *J Clim* 23(23):6312–6335. doi:[10.1175/2010JCLI3679.1](https://doi.org/10.1175/2010JCLI3679.1)
- WCRP (2000) Intercomparison and validation of ocean-atmosphere energy flux fields. final report of the Joint WCRP/SCOR Working Group on Air-Sea Fluxes (SCOR Working Group 110). Tech. Rep. WCRP-112 (WMO/TD-1036), World Meteorological Organization, World Climate Research Programme, Geneva, Switzerland
- Xin XG, Wu TW, Zhang J (2013) Introduction of CMIP5 experiments carried out with the climate system models of Beijing Climate Center. *Adv Clim Change Res* 4(1):41–49
- Xu Z, Chang P, Richter I, Kim W, Tang G (2014a) Diagnosing southeast tropical Atlantic SST and ocean circulation biases in the CMIP5 ensemble. *Clim Dyn* 43:3123–3145. doi:[10.1007/s00382-014-2247-9](https://doi.org/10.1007/s00382-014-2247-9)
- Yukimoto S, Adachi Y, Hosaka M, Sakami T, Yoshimura H, Hirabara M, Tanaka TY, Shindo E, Tsujino H, Delushi M, Mizuta R, Yabu S, Obata A, Nakano H, Koshiro T, Ose T, Kitch A (2012) A new global climate model of the Meteorological Research Institute: MRI-CGCM3 model description and basic performance. *J Meteorol Soc Jpn* 90A:2364
- Zheng Y, Shinoda T, Lin JL, Kiladis GN (2011) Sea Surface Temperature Biases under the Stratus Cloud Deck in the Southeast Pacific Ocean in 19 IPCC AR4 Coupled general circulation models. *J Clim* 24:4139–4164. doi:[10.1175/2011JCLI4172.1](https://doi.org/10.1175/2011JCLI4172.1)